ENERGY STORAGE IN *CHLAMYDOMONAS REINHARDTII* MEASURED WITH PHOTOACOUSTIC TECHNIQUES

By

CHENGYI YAN

A thesis submitted to the

Graduate School-New Brunswick

Rutgers, The State University of New Jersey

in partial fulfillment of the requirements

for the degree of

Master of Science

Graduate Program in Oceanography

written under the direction of

Paul G. Falkowski

and approved by

_____

_____

_____

New Brunswick, New Jersey

[October, 2009]

ABSTRACT OF THE THESIS

By CHENGYI YAN

Thesis Director:

Paul G. Falkowski

The energy storage efficiencies of the reaction centers in the intact cells of *Chlamydomonas reinhardtii* wild type cell, PSI-less mutants and PSII-less mutants in microsecond time window were determined using pulsed, time-resolved photoacoustic techniques. The heat emission from the photochemical reaction can result in the positive thermal expansion photoacoustic signal, opposing the negative thylokoid volume contraction signal caused by electrostriction during the charge separation. In this present research, we observed that PSI differed strongly from PSII, both in thermal expansion and volume contraction. Similar to the bacterial reaction centre, PSI is marked with the large volume contraction but small thermal expansion, in contrast to the large thermal expansion but small volume contraction in PSII. For wild type, the volume contraction signal is dominant over the thermal expansion signal upon low pulse energy illumination at room temperature. In microsecond time scale, the energy storage efficiencies were estimated to be 36%, 80±5%, and 50±14% per trap in wild type, PSI and PSII,

respectively. The different energy conversion efficiencies are probably attributed to the escape of the bound counterions from the particle surface in PSI and rapid electron transfer in PSII. In the present work, we conducted the photoacoustic experiments to study the energy storage in different photosystem with the intact cells of PSI-less and PSII-less mutants, instead of using either specific wavelength excitation light or PSII inhibitors (e. g. DCMU), which were commonly applied in the previous studies. We also proved photoacoustic techniques' usefulness and convenience in the photosynthesis research, especially in electron transfer and some related thermodynamics studies.

Acknowledgements

First and foremost I would like to thank my advisor, Dr. Paul G. Falkowski. Without his advices and supports, it would not be a complete thesis. I appreciate all that I have learned from him both in the lab and conversations. He is the person who brings me from China to America, to Rutgers, and I would have never doubted that it was a great honor to work with him in the past three years.

Also, I very deeply appreciate Dr. Maxim Gorbunov for his constructive advices and instruction through every stage of my research. Especially, I would like to thank him for his mental and physical support during my first cruise cross Atlantic Ocean on August 2008, when I had a bad time in seasickness.

Moreover, I would like to express my deep gratitude to Dr. Oscar Schofield, Dr. David Mauzerall, and Dr. Zvy Dubinsky for their suggestions that do improve my thesis, both structurally and logically.

My research could not have been completed without the help of the entire Environmental Biophysics and Molecular Ecology group. Thank you for all your help with samples and lab work.

In addition, this research was supported by Bi-National Science Foundation Grants 2002396. And my graduate studies were funded by the Institute of Marine and Coastal Sciences, Rutgers.

Finally, I want to thank my family who cares me with love and support, especially my wife Kejia for her consideration, patience, and sacrifice.

Table of Contents

List of tables

List of figures

I. Introduction

1.1 History of the photoacoustic effect

Photoacoustic (PA) effect was first discovered by Alexander Graham Bell in his search for a means of wireless communication in 1880 (Bell 1880; Lüscher 1984). In working with the photophone, Bell was surprised to find that sound could be produced by exposing optically absorbing materials to interrupted sun light, typically at the frequency of kHz. Bell applied this concept in developing "spectrophone", essentially an ordinary spectroscope equipped with a hearing tube instead of an eyepiece (Fig. 1) (Lüscher 1984). Samples could then be analyzed by sound when a source of light was applied.

In general, the PA effect is a conversion between light and acoustic waves due to absorption and localized thermal expansion. As showing in Fig. 2, when rapid pulses of light are incident on a sample of matter, they can be absorbed. It will stimulate a molecule to "jump" to its excited electronic state. Then the molecule will return to its ground state. In doing so, the resulting energy will be partially radiated as heat, which can warm the surrounding medium and lead to thermal volume expansion. Consequently, a pressure wave that can be detected as a PA signal is generated.

As noted by Bell, "the ear cannot of course compete with the eye for accuracy" (Production of sound by radiant energy, 1881), when examining the visible spectrum. He recognized that the PA effect had potential applications in spectroscopy. With the invention of the microphone and laser, Bell's dream became true and PA effect took on

new life as an important tool in spectroscopic analysis and continued to be applied in an increasing number of fields, including the photosynthesis research. Although PA spectroscopy first came out as a technique for photosynthesis research more than 30 years ago (Callis et al. 1972; Cahen et al. 1978; Malkin & Cahen 1979), so far it is not as popular as fluorescence or absorption photometry. PA techniques continue to show uncertainties today even though the nature of its signals is almost mastered and the methodological improvements are quickly accumulated. However, PA method shows its convenience and usefulness in the photosynthesis research. For example, oxygen evolution by leaf tissue can be measured photoacoustically with a specific time resolution which can not be matched by other methods (Malkin 1998). The storage of energy by electron transport also can be measured by PA system so as to allow the studies on cyclic electron transport pathway that is invisible to gas exchange and fluorescence techniques (Charlebois & Mauzerall 1999; Van Thor et al. 2000). In addition, PA techniques may detect light-induced conformational changes in isolated photosystem and other photochemically active proteins (Edens et al. 2000), which can be further applied in "postgenomics" biology, a subject attracting much attention today.

1.2 Characteristics of photosystems

Oxygenic photosynthesis in plants, eukaryotic algae and cyanobacteria is the basic energy conversion process on earth. This process is driven by two large protein cofactor complexes, photosystem I (PSI) and photosystem II (PSII), located in the thylakoid membrane, and this process involves a variety of electron-transfer reactions proceeding on the time scales from picoseconds to milliseconds. The photosystems utilize the absorbed light energy to translocate electrons across the membrane along the electron

transfer chain (ETC), thus generating a transmembrane gradient in both the electrical potential and proton concentration. Such gradients stimulate synthesis of ATP and reduction of $NADP^+$ to NADPH (Jordan et al. 2001), which, in turn, are used to convert CO_2 into carbohydrates in the subsequent dark reactions (Nugent 1996; Brettel 1997). The crystal structure of PSI from the thermophilic cyanobacterium *Synechococcus elongatus* revealed that PSI consists of 12 protein subunits and 127 cofactors (Jordan et al. 2001). The ETC in PSI includes the cofactors A_0 (*Chla*), A_1 (phylloquinone) and the Fe_4S_4 clusters F_X, F_A and F_B (Brettel 1997). The electron transfer is initiated by the excitation of the chlorophyll dimer P700 during the primary charge separation and then the electron is guided to A_0 and then A_1. At the cytoplasmic side, F_B donates the electron to ferredoxin (or flavodoxin) and then transfer to $NADP^+$ reductase. The reaction cycle is completed by re-reduction of $P700^+$ by cytochrome *c6* (or plastocyanin) at the lumenal side of the membrane. The electron carried by cytochrome *c6* is supplied by PSII from a pool of plastoquinones and the cytochrome b6/f complex (Jordan et. al 2001).

The first three-dimensional structure of a water-oxidizing PSII complex showed that it consists of more than 19 subunits (Zouni et al. 2001). The core of PSII is comprised by D1 and D2 proteins that bind P680 (*Chla*; primary electron donor), pheophytin (primary acceptor), Y_Z, the tyrosine electron donor to $P680^+$, and Q_A and Q_B (the first and secondary quinone acceptors). The ETC in PSII starts with transfer of an electron from the excited P680 in the luminal membrane to form cationic radical P680s during charge separation. Then the electron is transferred from a pheophytin to the first stable acceptor Q_A. After four successive steps of charge separation, P680 can extract four electrons from a Mn-cluster via TyrZ and accumulate four positive charges that are required to split

water and evolve one O_2 molecule and four H^+. Double reduced Q_B can acquire two H^+ to form Q_BH_2 that is released into plastoquinone pool. Q_B is replenished from the pool and ready for another cycle (Zouni et al. 2001).

1.3 Photoacoustic effect in photosynthesis

Generally, the light energy absorbed by the photosynthetic antennae pigments can be utilized or dissipated via three competing pathways including photochemical energy storage (~30%), loss as heat (~70%), and emission as *chlorophyll-a* fluorescence (~2%) (Kitajima & Butler 1975). The increase in photosynthetic efficiency is paralleled with the decrease in *Chl* fluorescence and thermal dissipation and *vice versa*. Fluorescence based techniques are extremely sensitive and widely used in photosynthesis research, however they only provide insight into PSII process, because *chlorophyll* fluorescence is originated almost entirely from PSII at room temperature (Krause and Weis 1991).

PA techniques measure the volume expansion that is produced by heating of the sample upon the absorption of light (Callis et al. 1972; Cahen et al. 1978; Malkin and Cahen 1979; Feitelson & Mauzerall, 1993; Mauzerall et al., 1995, 1998; Malkin, 1996).Inherently, this approach provides a potential to directly assess the overall thermal dissipation in photosynthetic reactions, including both PSII and PSI (Malkin and Canaani 1994). In spite of simple theory (Braslavsky and Heibel 1992; Fork and Herbert 1993; Malkin and Canaani 1994; McClean et al. 1998; Herbert et al. 2000; Delosme 2003), practical applications of the photoacoustic techniques in photosynthesis research and

ecophysiology remain limited by several factors related to the complexity of involved biophysical processes, the cost of existing laser-based PA systems, and low sensitivity of the techniques. Firstly, absorption and conversion of light energy in photosynthetic reactions may lead to negative volume change due to contraction of photosynthetic units under influence of electrostatic force induced by separated charges. This effect, called electrostriction, is superimposed on the thermal expansion PA signal (Braslavsky and Heibel 1992; Fork and Herbert 1993; Malkin and Canaani 1994; McClean et al. 1998; Herbert et al. 2000; Delosme 2003). Secondly, the quantitative interpretation of the PA signals requires the knowledge of the thermal expansion coefficient of the medium. Although most of the PA signals from a suspension of algae is due to thermal expansion of water (Braslavsky and Heibel 1992; Fork and Herbert 1993; Malkin and Canaani 1994; McClean et al. 1998; Herbert et al. 2000; Delosme 2003), the cellular compounds (lipids and proteins) with different thermal expansion properties may contribute to the PA signal (called "cell" artifact) that further complicates the processing of PA signals (Boichenko et. al 2001). The laser-based time-resolved PA techniques are mostly used for assessment of biophysical properties of isolated PSI and PSII complexes, as well as the small algal cells, cyanbacteria, which exhibit minor contribution of the "cell" artifact. The contribution of the "cell" artifact in larger phytoplankton cells remains unknown.

1.4 Different photoacoustic systems

Both the heat release and the electrostriction of reaction centers (RCs) can suddenly expand or shrink of the surrounding medium and induce pressure changes that can be

detected either in a gaseous phase by a microphone or in an aqueous phase by a piezoelectric transducer (Brunfeld et al. 1999). In gaseous medium, the photothermal signal is interfered with a photobaric signal which is caused by photochemical release or consumption of gas, i.e. O_2 in photosynthesis. Since heat diffusion through biological samples is much faster than that through gas (Poulet et al. 1983; Mauzerall 1990), the photobaric and photothermal signals can be separated kinetically. In the aqueous medium, the photothermal expansion signal can be combined with a volume contraction signal that is mainly due to electrostriction during the charge separation of RCs (Borsarelli and Braslavsky1998, 1999; Losi et al. 1999; Wegewijs et al. 1998). These two types of signals can be separated by comparison of the measurements at different temperature (Callis et al. 1972; Arata and Parson 1981; Delosme et al. 1994; Edens et al. 2000). Based on the type of light resources, photoacoustic systems are generally divided into two classes: continuously modulated and pulsed. Continuously modulated PA system uses a measuring light that is continuously modulated at frequencies ranging from 1 Hz to 1 kHz by means of a mechanical chopper or flashing LEDs (Herbert et al. 2000). It is best suited to measure the slow induction phenomena and photosynthesis in the steady state due to the continuously modeulated PA system's low time resolution (~ a few seconds) (Buschmann 1987; Snel et al. 1990). Pulsed PA system uses short pulses of light from lasers or LEDs and piezoelectric detectors to record the PA waves. It can achieve higher time resolution down to microsecond scale (Peters and Snyder 1988; Nitsch et al. 1988; Bruce and Salehian 1992; Delsome et al. 1994; McClean et al. 1998) and allow measurement of fast induction phenomena, including S states of the oxygen evolving complex in leaf tissue (Canaani et al. 1988; Mauzerall 1990), the earliest steps of

photosynthetic electron transport in photosystems (Callis et al. 1972; Arata and Parson 1981; Delosme et al. 1994; Delosme 1998; Edens et al. 2000; Boichenko et al. 2001; Hou et al. 2001a, b), and energy storage (ES), i.e. the ratio of the energy stored in the photochemical products to the absorbed energy (Malkin and Canaani 1994; Boichenko et al. 2001; Hou et al. 2001a, b). Pulsed PA system also can measure the steady state photosynthesis in intact cells and leaf tissues with illumination by both the pulse and continuous background light (Kolbowski et. al 1990; Boichenko et al. 2001; Hou et al. 2001a, b). In particular, the relative ES efficiency in PSI was found to be >70% in both the isolated particles (Nitsch et al. 1988) and intact cyanobacterial cells (Mullineaux et al. 1991; Bruce and Salehian 1992).

1.5 Objectives

To estimate the photoacoustically energy storage efficiencies in PSI and PSII, the previous studies commonly used either specific wavelength excitation light for each photosystem or PSII inhibitors such as DCMU (Cha & Mauzerall 1992). In the present study, we applied a modified microsecond time-resolved PA system to assess the ES for each photosystem in intact cells of the green alga *Chlamydomonas reinhardti* and its PSI- and PSII-deficient mutants. It requires corrections for cell artifact brought by the heterogeneous system (Boichenko et. al 2001), although the magnitude of cell artifact is small in isolated PS complexes and small cells.

II. Material and Methods

2.1 Culture growth condition

All the *Chlamydomonas reinhardtii* cultures were provided by the *Chlamydomonas* Center in Duke University. In addition to the control wild type (WT) culture (CC-125), we chose CC-4134 and CC-1042 as the PSI-less mutants, CC-4151 and CC-1051 as the PSII-less mutants. After the cells' growth in the solid culture medium for 5 days, we transferred the dense cells to 500 ml flasks that contain the liquid Sueoka's High Salt medium (Sueoka 1960) at pH 7.0 and 25 °C. The algal cells were cultured under a saturating light which was alternately provided between light and dark phases with a 12 hours interval. The light was supplied by using cool-white fluorescent lamps with 200 $\mu Em^{-2}s^{-1}$ intensity for the WT culture and 50 $\mu Em^{-2}s^{-1}$ intensity for the mutant cultures, respectively. All cultures were bubbled with filtered CO_2-enriched air (5% CO_2). Light intensity was measured with a Li-Cor quantum/radiometer (LI-185B, Li-Cor Inc., Lincoln, USA). Cell proliferation was determined by cell numbers. Algal cells were harvested at the late exponential phase (about 8.0×10^6 cells ml^{-1}) by centrifugation at 2000×*g* for 5 minutes and washed 5 times with High Salt medium. The cells were re-suspended in the High Salt medium at a concentration of 1.5×10^6 cells ml^{-1} for experiments.

2.2 Low-temperature fluorescence spectroscopy

The cells were adapted in the dark for 20 minutes before measurement. Samples were frozen in a liquid nitrogen Dewar vessel under dim green light. Fluorescence emission spectra corrected with quantum were measured at 77 K with an SLM/Aminco 4800 spectrofluorometer (Rochester, NY) using an internal standard and equipped with a low-temperature accessory. For measurement of emission spectra, the slit width of excitation monochromator was set to 4 nm at a wavelength of 435 nm and the spectra were captured from 650 nm to 800 nm. The spectra were corrected for wavelength-dependent sensitivity of the instrument. Using a peak-fitting program, the total emission spectra were deconvoluted into three to five component bands, assuming the Gaussian distribution of the excited states (Mimuro et al.1982).

2.3 Photoacoustic apparatus

The procedure of the pulse time-resolved photoacoustic measument is similar to the methodology described elsewhere (Feitelson & Mauzerall 1996; Edens et al. 2000; Hou et al. 2001a, b; Boichenko et al. 2001; Pinchasov et al. 2005, 2007). In the present study, we used the 7 ultra-bright Light Emitting Diodes (LEDs, Lumileds Co., Star III) as the light source, which allowed us to build a compact and user-friendly system that could be potentially used for field studies, in contrast to the laser as the light source. The LEDs emitted flashes of red light with 640 nm central wavelength, 30 nm bandwidth and adjustable duration ranging from 1 μs to 100μs. The optimal flash duration was found to

be ca. 8 μs for the particular detector, which was selected by matching the oscillation semi-period of the piezo-acoustic sensor (personal communication with Dr. Gorbunov). A suite of CW blue ultra-bright LEDs was incorporated into the optical flasher to provide a source of saturating illumination. Excitation light was focused into the sample cuvette by a Fresnel lens with 10 cm focal length, 12 cm diameter and 3 cm spot size. The coupled photoacoustic/fluorescence cell incorporated a custom-built quartz cuvette with 1 cm optical path and 50 cm diameter. It had a high-reflective dielectric mirror that was optimized for the red spectral region (99% reflection for 600-700 nm, Newport), and a custom-built microphone detector that contained a 128 μm ceramic Lead Zirconite Titanates piezo disk via a stainless steel holder according to the design of Arnaut et al. 1992. The pulse was incident upon the suspension of algae whose pigments (chlorophyll, carotenoid or phycobilin) absorbed part of the laser light. A variable fraction of the absorbed light energy was converted and stored in the photochemical products. The majority of residual energy was emitted as heat and then produced rhythmic pressure changes that can be sensed by the piezo-detector (for details see Pinchasov et al. 2005). The signals from the piezoelectric disc were amplified by an Amtek A-250 preamplifier, filtered to pass 3 kHz/400 kHz, and further amplified by SRS 560 preamplifier. The signals were accumulated over a preset number of flashes and spectrally analyzed with an incorporated FFT (Fast Fourier Transform) procedure before digitized by a Tektronix TDS 430A oscilloscope. The PA data were stored and analyzed on a computer subsequently. The schematic design of the PA experimental system is shown in Fig. 3 (Pinchasov et al. 2007). The real PA experimental system we used in the present research is shown in Fig. 4.

III. Results

3.1 Low-temperature fluorescence spectra

In order to estimate the relative abundance of PSI and PSII in WT cell and mutants, we measured chlorophyll fluorescence emission spectra of the samples at 77K. When excited at 435 nm, the spectra of wild type displayed two major peaks at approximately 718 nm and 685 nm and a shoulder at 749 nm (Fig. 5a). The excitation signature for the 685-nm emission band was virtually identical in both WT and all the mutants while the 718-nm was apparently drift left to approximately 710 nm in both two PSII-less mutants. Analytical decomposition of the fluorescence emission spectra by means of the peak fitting method is shown in Figure 5. The analysis revealed the presence of four components in the spectrum of WT cells with peaks at 686, 698, 718, and 749 nm (Fig. 5a). The same analysis method was applied to the mutants' data. For the PSI-less mutants, the spectrum of strain CC-4134 cells contained four components with peaks at 686, 696, 715, and 755nm (Fig. 5b); the spectrum of strain CC-1042 cells contained five fluorescence bands with peak at 684, 698, 717, 745, and 761 nm (Fig. 5c). For the PSII-less mutants, there were three fluorescence bands with peaks at 688, 710 and 741 nm in the spectrum of strain CC-4151 cells (Fig. 5d), in contrast to the two distinct components with peaks at 688 and 710 nm in the spectrum of strain CC-1051 cells (Fig. 5e).

The intensity of the fluorescence emission due to PSI and PSII can be used to estimate

the abundance of PSI and PSII in green algal cells. Two fluorescence bands, F685 and F695, are generally derived from PSII core antenna pigment proteins, CP43 and CP47, respectively (Krause and Weis 1991), whereas the longer wavelength band, F710–735, is ascribed to PSI antenna pigments (Murata et al. 1966). The characteristics of the component bands and PSI/PSII stoichiometries are originated from PSII (F685 and F695). 77K fluorescence emission spectra of PSI (F_{PSI}) are summarized in Table 1. Notably, two PSII-less mutants lack the F695 component (Fig 5d & e, Table 1), which confirms the lack of PSII core complex. For different types of cells, the emission peaks of PSI fluorescence visibly vary between 710 nm to 735 nm (718, 715, 717, and 710 nm), but the emission peaks of PSII are fairly constant at approximately 685 nm and 695 nm, respectively. All the mutants in the present work were not pure. Compared with strain CC-4134, strain CC-1042 was more perfect with less PSI (~20% of PSI). In term of PSII content, strain CC-1051 (9.1% of PSII) was better than CC-4151 (21.9% of PSII) (Table 1). The PSI- or PSII-less mutant also can be easily distinguished with its ratio of PSI/PSII (table 1).

3.2 Photoacoustic signal's nature and separation

In contrast to intact leaves, photobaric gas signal (O_2) does not contribute to PA signals (within ±2%) in aqueous solution (e.g., suspension of phytoplankton cells) due to the thick water layer in the sample at the fast frequency (Cha & Mauzerall 1992). Therefore, the PA signal entirely attributes to thermal expansion and/or electrostriction. The volume contraction generates a negative pressure, opposing the positive pressure of the expansion

signal, which results in 180 degree phase shift between those two signals. We used a carbon black ink as an external calorimetric reference, which was adjusted to the same optical density as the sample at a given wavelength in the same buffer medium. It can degrade absorbed photons into heat much faster than the resolution time (Boichenko et al. 2001). We used the internal calorimetric reference upon saturating background illumination when the heat emission was entirely caused by closed photosynthetic RCs (Boichenko et al. 2001). Low flux was applied to excite the samples because of their large optical cross section *in vivo*. The separation of thermal expansion component relies on measurements at the temperature of maximum water density (~ 4°C), depending on the presence of dissolved salts (Callis et al. 1972; Arata and Parson 1981; Delosme et al. 1994; Edens et al. 2000). Since the thermal expansion of water is zero ($\delta V/\delta T=0$) at 4°C while the electrostriction is temperature independent in its biological range (Malkin et al. 1994), the thermal expansion signal will be abolished and therefore the sole electrostriction component remained in the PA spectrum at 4°C. Alternatively, the contribution of electrostriction varies dramatically with the state of RCs, maximizing at fully opened RCs and minimizing to zero when the RCs are closed under saturating background illumination (Hou et al. 2001 a, b). Therefore, PA spectrum will only contain the thermal expansion signal under saturating background illumination. The comparison of the measurements at different temperatures and different illumination states provides a background to separate the thermal expansion and electrostriction in PA spectrum. Figure 6 indicates the typical PA wave from the WT cells and reference carbon ink. When the RCs were closed due to saturating background light illumination, a positive photoacoustic signal was observed at 25 °C (Figure 6, curves 1). It had the same shape and phase as the

signal from a dilute solution of carbon ink (Figure 6, curves 5). In contrast, the signal of open RCs (Figure 6, curve 3) was shifted by 180 degree, which is indicative of the overall negative volume contraction change and the dominance of electrostriction component in the signal. A negative wave with larger amplitude was created in weak pulse light condition at ~4°C (Figure 6, curve 2). Upon excitation of the RCs with a saturating background light at ~4°C, a weak wave was observed (Figure 6, curve 4). A neglectable PA signal (Figure 6, curve 6) was observed from carbon ink when it was kept at weak pulse light and ~4°C.

In the heterogeneous intact cells, thermal expansion coefficient of cellular materials is different from the surrounding water, which leads to some "artifact" in PA spectra under continuous saturating light excitation at ~4°C (curve 4 in Fig. 6). We corrected all other three PA curves with this "artifact" (see below for detail) and then smoothed them with FFT filter function of Origin 6.0 program. All the PA spectra are demonstrated in Fig. 7. The PA spectra of both PSI-less mutants, strain CC-4134 and CC-1042, have distinctly different patterns with that of PSII-less mutants, strain CC-4151 and CC-1051 which are similar with that of WT cells (Fig. 6). As described in Material and Method, Curve 1 refers to the PA signal observed at 25°C with continuous saturating background light, which is the pure thermal expansion signal. Curve 2 is the PA signal produced under weak pulse background light at ~4°C , which should be the pure electrostriction signal. Curve 3 is the combined PA signal, both thermal expansion and electrostriction, which is generated under weak pulse background light at 25°C. Apparently, electrostriction is dominant over thermal expansion in PSII-less mutants (Fig 7a & 7b), which implies that

the electron transfer through the thylakoid membrane more frequently in PSI than in PSII. Thermal expansion is dominant over electrostriction in PSI-less mutants (Fig 7c & 7d), which indicates that PSII is the major site for heat dissipation in contrast to PSI. Similar with the PSII-less mutants, negative (contractive) PA signal was observed in the microsecond time window from the competent RCs in intact cells even at room temperature under low energy trains of laser pulses (Fig 6, curve 3), which implicates that contraction volume change caused by PSI is larger than that was caused by PSII. The PA signal of PSI-less mutants represented a volume contraction at ~4 °C but a thermal expansion at 25°C. This observation of PSI-less mutants was different from that of PSII-less mutants and that of bacterial RCs from *Rb. Sphaeroides* (Edens et al. 2000), which presented negative signals even at room temperature. This implies that the heat emission of electron transfer in PSII is larger and/or the contraction volume change is smaller than that in PSI.

3.3 Energy storage of different photosystem

The processing of PA signal requires a correction for any fluorescence emission, the prompt heat loss, and the immediate heat release, when the incident energy is beyond the trap energy (Cha & Mauzerall 1992; Malkin & Canaani 1994). These corrections are often negligible at the present error levels. The heat diffusion in the cell matrix allows it to thermally expand until it was cooled down by the surrounding water. Thus, this heterogeneous artifact depends on the cell size (Boichenko et al. 2001). If the thermal relaxation time of the absorbent is longer than the resolution time of the PA detection

system or in the uniform solution, the cell artifact will disappear. In present work, we used the equation (8) proposed by Boichenko et al. (2001) to correct such "artifact" and calculate the ES.

$$ESm = \frac{PAm - PAo}{PAm} = 1 - \frac{PAo}{PAm} \qquad (1)$$

$$\frac{PAo}{PAm} = \frac{PAo(25) - PAo(4)}{PAm(25) - PAm(4)} \qquad (2)$$

Here, ES_m is the maximum ES efficiency instead of the maximum rate of ES in sample; PAm is the amplitude of PA signal produced when RCs are closed under the continuous saturating light condition. The majority of absorbed energy (~75%) is emitted as heat because all the RCs are closed. Under this circumstance, PA signal reaches the maximum level and it also can serve as the internal calorimetric reference and provide the photochemically 'inactive' reference value from the same sample in which ES is being measured (Callis et al. 1972; Lasser-Ross et al. 1980); PAo is the amplitude of PA signal generated in the weak pulse light condition. All the RCs are open for photochemical reaction; therefore the heat loss is minimal. PAo(25) refers to the amplitude of PA signal generated under weak pulse light at 25 °C (Fig. 6, curve 4), which is the combined PA signal due to both contraction volume change, thermal expansion and cellular "artifact"; PAo(4) is the amplitude of PA signal produced under weak pulse light at 4 °C (Fig.6, curve 2), which attributes to the contraction volume change and cellular "artifact"; PAm(25) is the amplitude of PA signal generated under continuous saturating background light at 25 °C (Fig.6, curve 1), caused by thermal expansion and cellular "artifact"; PAm(4) is the amplitude of PA signal generated under continuous saturating

background light at 4 °C. (Fig. 6, curve 3), which is the pure signal produced only by cellular "artifact". Due to low signal-to-noise ratio, we smoothed the PA data and normalized them according to equation (2). The PAo and PAm signal spectra of different types of cells are summarized in Fig. 8. We noticed that the cell artifact was relatively small in spite of large cell size.

Visibly, WT and PSI-less mutant CC-1042 have relatively high PAo. It indicates that these cells have relatively low ES because large portion of energy is emitted as heat instead of photochemical storage. In contrast, both PSII-less mutants (CC-4151 and CC-1051) have high ES. Combined equation (1) and (2), the real ES can be calculated as follow:

$$ESm = 1 - \frac{PAo(25) - PAo(4)}{PAm(25) - PAm(4)} \qquad (3)$$

ES efficiencies we obtained are listed in table 2. The ES efficiencies per absorbed quantum on the microsecond time scale were estimated to be 36%, 80±5%, and 50±14% per trap in WT, PSI and PSII, respectively. There is a good agreement between the results of us and those of Boichenko et al. 2001. They proposed that ~80% and ~45% per trap for PSI and PSII in the intact cells of the cyanobacterium *Synechocystis PCC 6803*, respectively. Additionally, similar ES efficiencies were confirmed in the isolated PSI and PSII complexes *in vitro* (Hou et. al 2001a & b). The photoacoustically ES efficiency within a certain time scale is an important parameter in defining the electron transport steps under observation. For example, it is about 40% on the millisecond time scale (Cha & Mauzerall 1992; Charlebois & Mauzerall 1999).

IV. Discussion

4.1 Confirmation of PSI-less and PSII-less mutant

Generally, long-wavelength fluorescence emissions at 77 K of vascular plants, red algae, green algae and cyanobacteria are composed of three major fluorescence bands, F685, F695, and F710–735 (Murata et al. 1966). The origin of each fluorescence band has been assigned to specific action spectra (Murata et al. 1966) that are obtained from the PSI and PSII complexes of purified spinach chloroplasts (Satoh 1980), and from PSI- or PSII-less mutants of cyanobacteria (Nilsson et al. 1992; Shen and Vermaas 1994). The 77K fluorescence results indicate that both CC-4134 and CC-1042 lack the PSI core complex, while mutants CC-4151 and CC-1051 lack the PSII core complex.

4.2 Different pattern of photoacoustic spectra

Our results revealed that PA profiles of PSI-less mutants with open RCs had a positive amplitude at 25°C but a negative amplitude at 4°C (Fig 7a and 7b), which implied that the PA signals contained a large thermal expansion signal and a small volume contraction signal. In contrast, PSII-less mutants showed a large negative amplitude at 25 °C and even larger at 4 °C (Fig 7c & 7d), which indicated that the PA signals contained a large volume contraction and a small thermal expansion. The thermal expansion signal reflects the enthalpy change in each individual photosystem. The enthalpy and volume change of PSI are similar to those of bacterial RCs of *Rb. Sphaeroides* (Edens et al. 2000) that is

supposed to be about the same as PSII. This result is surprising because the structure and organization of PSII are believed to be similar to that of bacterial RCs (Trebst 1986; Michel and Deisenhofer 1998; Lancaster et al. 2000; Zouni el al. 2001). The volume contraction of RCs of PSII-less mutants is directly caused by the formation of $P_{700}^{+}F_A/F_B^{-}$ from the excited-state P_{700}^{*} during the light-induced charge separation in microsecond time window (Nugent 1996; Golbeck 1994; Brettel 1997; Diner and Babcock 1998; Hou et al. 2001a). Similar to the bacterial RCs (Yeate et al. 1987), there are excess charges (+13) on the A1 side and (-1) on the P700 side of membranes respectively (Hou et al. 2001a). These charges favor the transmembrane electron transfer and thence they can be cancelled by the electron transfer, leading to the liberation of some counterions that are originally bound with charges. The escape of such counterions can result in the large volume change in PSI (Hou et al. 2001a).

Moreover, a much smaller volume contraction in PSII compared to PSI was observed in the isolated core complexes *in vitro* (Hou et al. 2001b). It should be noticed that the variation of volume change in both PSI (Hou et al. 2001a) and PSII (Hou et al. 2001b) was not caused by a low quantum yield since the quantum yield was close to unity in the experiment. The large enthalpy change in PSII may be generated by the rapid proton-transfer step associated with the electron transfer. The electron-transfer rate in Mn-depleted PSII core complexes depends on the pH of the solution. And the ES in PSII also is dependent on pH (Hou et. al 2001b). A more polar environment in the PSII complex can drive the electron transfer faster, leading to relatively higher heat emission (Hou et al. 2001b). The weak contraction of PSII RCs is probably due to the fast electron

transfer from Y_Z^- to $P680^+$ and cancellation of the charges of the pair due to proton emission (Diner & Babcock 1996; Hou et al. 2001b). Nevertheless, the liberation of counterions by charge neutralization in PSI does not occur in PSII since there is no charge formation on the microsecond time scale (Hou et al. 2001b).

4.3 Explanation of different energy storage efficiency

The ES efficiency depends on the early steps of electron transport occurring within the RCs. In the microsecond time window, separated charges should be stabilized mainly in states $Y_Z^*P680Q_A^-$ for PSI-less mutants or PSII complex and $P_{700}^+F_A/F_B^-$ for PSII-less mutant or PSI complex, respectively (Golbeck 1994; Nugent 1996; Brettel 1997; Diner & Babcock 1998; Hou et al. 2001b). Contrary to previous thoughts, our results show that PSII-less mutants have very high ES efficiency (~80%) in contrast to PSI-less mutants (~50%), indicating a significant contribution to the ES by cyclic electron flow that is mediated by PSI, compared with the linear electron flow that involves both PSII and PSI. Delsome et al. (1994) suggested that relatively poor ES efficiency in PSII resulted from the large energy losses in the PSII antenna, which is confirmed by our results here. A larger thermal expansion signal in PSII implies a larger heat loss in PSII than in PSI, which therefore depress the ES in photochemical products.

V. Conclusion and Extension

Our study clearly demonstrated the power and convenience of photoacoustic techniques in measuring the photosynthetic ES efficiency of green algae. Generally, PSI complex can convert more absorbed energy into photochemical products (~80%) than PSII complex (~45%). The difference of ES efficiency possibly was caused by the escape of the bound counterions from the particle surface in PSI and rapid electron transfer in PSII (Hou et al. 2001 a, b; Boichenko et al. 2001). In addition, the light-induced contraction of RCs presented by the PA spectra can be used as a quantitative indicator of charge separation (Delosme et al. 1994); consequently, it can provide the direct information about the electron transfer. Furthermore, the information presented by the electrostriction data can be applied as an internal reference for the dielectric coefficient of the protein in the RCs and local compressibility of the medium (Mauzerall et al. 1995; Edens et al. 2000). Surprisingly, it offers us a novel way to understand the reaction dynamics of many photochemically active proteins (McClean et al. 1998). PA can be further applied in "postgenomics" biology, a subject attracting much attention today.

In the future, we should be dedicated to find the best way to accurately calibrate the quantitative photoacoustic signals and improve photoacoustic instrument's sensitivity, so that it can contribute more to the photosynthesis research by complementing the fluorescence and absorption methods. Meanwhile, the developments of technique and methodology in the photoacoustic system, such as the use of microphotoacoustic spectrometer in the study of protein dynamics, are also taking place increasingly (Herbert et al. 2000).

VI. References

Arata H and Parson WW (1981) Enthalpy and volume changes accompanying electron transfer from P-870 to quinones in *Rhodopseudomonas sphaeroides* reaction centers. *Biochim Biophys Acta* 636: 70–81.

Arnaut LG, Caldwell RA, Elbert JE and Melton LA (1992) Recent advances in photoacoustic calorimetry*:* Theoretical basis and improvements in experimental *design. Re*V. *Sci*. *Instrum*. 63: 5381-5389.

Bell AG (1880) Am. J. Sci. 20: 305–324.

Boichenko VA, Hou JM and Mauzerall DC (2001) Thermodynamics of electron transfer in oxygenic photosynthetic reaction centers: volume change, enthalpy, and entropy of electron-transfer reactions in the intact cells of the cyanobacterium *Synechocystis* PCC 6803. *Biochemistry* 40: 7126-7132.

Borsarelli C and Braslavsky SE (1998) Volume changes correlate with enthalpy changes during the photoinduced formation of the ^{3}MLCT state of Ruthenium(II) bipyridine cyano complexes in the presence of salts. A case of the entropy−enthalpy compensation effect. *J. Phys. Chem. B* 102:6231-6238.

Borsarelli C and Braslavsky SE (1999) Enthalpy, volume, and entropy changes associated with the electron transfer reaction between the ^{3}MLCT State of $Ru(Bpy)_3^{2+}$ and methyl viologen cation in aqueous solutions. *J. Phys. Chem. A* 103: 1719-1727.

Braslavsky SE and Heibel GE (1992) Time-resolved photothermal and photoacoustic methods applied to photoinduced processes in solution. *Chem Rev* 92: 1381–1410

Brettel K (1997) Electron transfer and redox-cofactors in photosystem I. *Biochim. Biophys. Acta* 1318: 322-373.

Bruce D and Salehian O (1992) Laser-induced optoacoustic calorimetry of cyanobacteria. The efficiency of primary photosynthetic processes on state 1 and state 2. *Biochim. Biophys. Acta 1100*: 242-250.

Brumfeld V, Nagyt L, Kiss V and Malkin S (1999) Wide-frequency Hydrophone Detection of Laser-induced Photoacoustic Signals in Photosynthesis. *Photochemistry and Photobiology.* 70(4): 607-615

Buschmann C (1987) Induction kinetics of heat emission before and after photoinhibition in cotyledons of *Raphanus sativus*. *Photosynth. Res.* 14: 229–240

Cahen D, Malkin S and Lerner EI (1978) Photoacoustic spectroscopy of chloroplast membranes: Listening to photosynthesis. *FEBS Lett.* 91: 339–342.

Callis JB, Parson WW and Goutermann MM (1972) Fast changes of enthalpy and volume on flash excitation of *Chromatium* chromatophores. *Biochim Biophys Acta* 267: 348–362.

Cha Y and Mauzerall DC (1992) Energy storage of linear and cyclic electron flows in photosynthesis. *Plant Physiol*. 100: 1869–1877.

Charlebois DO and Mauzerall DC (1999) Energy storage and optical cross-section of PS I in The cyanobacterium *Synechococcus PCC* 7002 and a psaE$^-$ mutant. *Photosynth. Res.* 59: 27-38.

Delosme R (2003) On some aspects of photosynthesis revealed by photoacoustic studies:a critical evaluation. *Photosynth. Res.* 76: 289–301.

Delosme R, Béal D and Joliot P (1994) Photoacoustic detection of flash-induced charge separation in photosynthetic systems: Spectral dependence of the quantum yield. *Biochimica et biophysica acta. Bioenergetics* 11: 56-64, Elsevier Science.

Diner BA and Babcock GT (1996) in *Oxygenic Photosynthesis: The Light Reactions* (Ort DR and Yocum CF, Eds.) pp 213-247, Kluwer Academic Publishers, Dordrecht, The Netherlands.

Edens GJ, Gunner MR, Xu G and Mauzerall DC (2000) The enthalpy and entropy of reaction for formation of P+ QA− from excited reaction centers of *Rhodobacter sphaeroides*. *J Am Chem Soc* 122: 1479–1485.

Feitelson J and Mauzerall DC (1993) Wide band timeresolved photoacoustic study of electron transfer reactions: Difference between measured enthalpy and redox free energies. *J. Phys. Chem.* 97: 8410–8413.

Feitelson J and Mauzerall DC (1996) Photoacoustic evaluation of volume and entropy changes in energy and electron transfer. triplet state porphyrin with oxygen and naphthoquinone-2-sulfonate. *J. Phys. Chem.* 100: 7698-7703.

Fork DC and Herbert SK (1993) The application of photoacoustic techniques to studies of photosynthesis. *Photochem Photobiol* 57: 207–220.

Golbeck JH (1994) in *The Molecular Biology of Cyanobacteria* (Bryant, D. A., Ed.) pp 319-360, Kluwer Academic Publishers, Dordrecht, The Netherlands.

Herbert SK, Han T and Vogelmann TC (2000) New applications of photoacoustics to the study of photosynthesis. *Photosynth. Res.* 66: 13–31.

Hou JM, Boichenko VA, Diner BA and Mauzerall DC (2001a) Thermodynamics of electron transfer in oxygenic photosynthetic reaction centers: volume change, enthalpy, and entropy of electron-transfer reactions in manganese-depleted Photosystem II core

complexes. *Biochemistry* 40: 7117-7125.

Hou JM, Boichenko VA, Wang YC, Chitnis PR and Mauzerall DC (2001b) Thermodynamics of electron transfer in oxygenic photosynthetic reaction centers: a pulsed photoacoustic study of electron transfer in Photosystem I reveals a similarity to bacterial reaction centers in both volume change and entropy. *Biochemistry* 40: 7109-7116.

Jordan P, Fromme P, Witt HT, Klukas O, Saenger W and Krauss N (2001) Three-dimensional structure of cyanobacterial photosystem I at 2.5 Å resolution. *Nature* 411: 909-917.

Kitajima M and Butler WL (1975) Quenching of chlorophyll fluorescence and primary photochemistry in chloroplasts by dibromothymoquinone. *Biochim. Biophys.* Acta. 376: 105–115.

Kolbowski J, Reising H and Schreiber U (1990) Computercontrolled pulse modulation system for analysis of photoacoustic signals in the time domain. *Photosynth. Res.* 25: 309–316.

Krause GH and Weis E (1991) Chlorophyll fluorescence and photosynthesis: the basics. *Annu Rev Plant Physiol Plant Mol Bio*l 42: 313-349.

Lancaster CRD, Bibikova MV, Sabatino P, Oesterhelt, D and Michel H (2000) Structural basis of the drastically increased initial electron transfer rate in the reaction center from a Rhodopseudomonas viridis mutant described at 2.00- Å resolution. *J. Biol. Chem.* 275: 39364-39368.

Lasser-Ross N, Malkin S and Cahen D (1980) Photoacoustic detection of photosynthetic activities in isolated broken chloroplasts. *Biochim Biophys Acta.* 593(2):330-341.

Losi A, Braslavsky SE, Gartner W and Spudich, JL (1999) Time-Resolved Absorption and Photothermal Measurements with Sensory Rhodopsin I from *Halobacterium salinarum. Biophys. J.* 76: 2183-2191.

Lüscher E (1984) Photoacoustic effect in condensed matter—historical development. in Lüscher E et al., eds. *Photoacoustic Effect: Principles and Applications.* Braunschweig: Friedr. Vieweg & Sohn, p. 1.

Malkin S (1996) The photoacoustic method in photosynthesis-monitoring and analysis of phenomena which lead to pressure changes following light excitation. In Amesz, J. & A. Hoff (eds), *Biophysical Techniques in Photosynthesis.* Kluwer Academic Publishers, Dordrecht, 191–206.

Malkin S (1998) Attenuation of the photobaric-photoacoustic signal in leaves by oxygen-consuming processes. *Isr J Chem* 38: 261–268.

Malkin S and Cahen D (1979) Photoacoustic spectroscopy and radiant energy conversion: Theory of the effect with special emphasis on photosynthesis. *Photochem Photobiol* 29: 803–813.

Malkin S and Canaani O (1994) The use and characteristics of the photoacoustic method in the study of photosynthesis. *Annu Rev Plant Physiol Plant Mol Biol* 45: 493–526.

Mauzerall DC (1990) Determination of oxygen emission and uptake by pulsed, time resolved photoacoustics. *Plant Physiol* 94: 278–283.

Mauzerall DC, Feitelson J and Dubinsky Z (1998) Discriminating between phytoplankton taxa by photoacoustics. *Isr J Chem* 38: 257–260.

Mauzerall DC, Feitelson J and Prince R (1995) Wide band, time–resolved photoacoustic study of electron transfer reactions: Difference between measured enthalpies and redox free energies. *J. Phys. Chem.* 99: 1090–1093.

Mauzerall DC, Gunner MR, and Zhang JW (1995) Volume contraction on photoexcitation of the reaction center from Rhodobacter sphaeroides R-26: internal probe of dielectrics. *Biophys. J. 68*, 275-280.

McClean MA, Di Primo C, Deprez E, Hoa GHB and Sligar SG (1998) Photoacoustic calorimetry of proteins. *Meth Enzymol* 295: 316–330.

Michel H and Deisenhofer J (1988) Relevance of the photosynthetic reaction center frompurple bacteria to the structure of photosystem II. *Biochemistry. 27*: 1-7.

Mimuro M, Murakami A and Fujita Y (1982) Studies on spectral characteristics of allophycocyanin isolated from *Anabaena cylindrica*: Curve-fitting analysis. *Arch Biochem Biophys* 215: 266–273.

Mullineaux CW, Griebenow S and Braslavsky SE (1991) Photosynthetic energy storage in cyanobacterial cells adapted to light-states 1 and 2. A laser-induced optoacoustic study. *Biochim. Biophys. Acta* 1060: 315-318.

Murata N, Nishimura M and Takamiya A (1966) Fluorescence of chlorophyll in photosynthetic systems. III. Emission and action spectra of fluorescence – three emission bands of chlorophyll *a* and the energy transfer between two pigment systems. *Biochim Biophys Acta* 126: 234–243.

Nilsson F, Simpson DJ, Jansson C and Andersson B (1992) Ultrastructural and biochemical characterization of a *Synechocystis* 6803 mutant with inactivated *psbA* genes. *Arch Biochim Biophys* 295: 340–347.

Nitsch C, Braslavsky SE and Schatz GH (1988) Laser-induced calorimetry of primary

processes in isolated photosystem I and photosystem II particles. *Biochim. Biophys. Acta 934*: 201-212.

Nugent JHA (1996) Electron transfer in Photosystem I and Photosystem II. *Eur. J. Biochem*. 237: 519-531.

Peters KS and Snyder GJ (1988) Time-resolved photoacoustic calorimetry: Probing the energetics and dynamics of fast chemical and biochemical reactions. *Science* 241: 1053–1057.

Pinchasov Y, Kotliarevsky D, Dubinsky Z, Mauzerall DC and Feitelson J (2005) Photoacoustics as a diagnostic tool for probing the physiological status of phytoplankton. *Israel Journal of Plant Sciences* 53: 1–10.

Pinchasov Y, Porat R, Zur B and Dubinsky Z (2007) Photoacoustics: a novel tool for the determination of photosynthetic energy storage efficiency in phytoplankton. *Hydrobiologia* 579:251–256.

Poulet P, Cahen D and Malkin S (1983) Photoacoustic detection of photosynthetic oxygen evolution from leaves-uantitative analysis by phase and amplitude measurements. *Biochim. Biophys. Acra.* 724: 433-446.

Production of Sound by Radiant Energy, *The Manufacturer and Builder.* (1881) Vol. 13, Issue 7. New York: Western & Co. p.156.

Satoh K (1980) F-695 emission from the purified Photosystem II chlorophyll *a*-protein complex. *FEBS Lett.* 110: 53–56.

Shen G and Vermaas WFJ (1994) Chlorophyll in a *Synechocystis* sp. PCC 6803 mutant without Photosystem I and Photosystem II core complexes. Evidence for peripheral antenna chlorophylls in cyanobacteria. *J Biol Chem* 269: 13904–13910.

Snel JFH, Kooijman M and Vredenberg WJ (1990) Correlation between chlorophyll fluorescence and photoacoustic signal transients in spinach leaves. *Photosynth. Res.* 25: 259–268.

Sueoka N (1960) Mitotic replication of deoxyribonucleic acid in *Chlamydomonas reinhardtii*. *PNAS* 46: 83-91.

Trebst A (1986) *Z. Naturforsch. 41c*, 240-245.

Van Thor JJ, Jeanjean R, Havaux M, Sjollema KA, Joset F, Hellingwerf KJ and Matthis HC (2000) Salt shock inducible Photosystem I cyclic electron transfer in *Synechocystis* PCC6803 relies on binding of ferredoxin:NADP(+) reductase to the thylakoid membranes via its CpcD phycobilisome linker homologous Nterminal domain. *Biochim Biophys Acta* 1457: 129–144.

Wegewijs B, Paddon-Row MN and Braslavsky SE (1998) Volume change associated with large photoinduced dipole formation in a rigid donor−acceptor compound: new approach to optoacoustic volume determination. *J. Phys. Chem. A.* 102: 8812-8818.

Yeates TO, Komiya H, Rees DC, Allen JP and Feher G (1987) Structure of the reaction center from Rhodobacter sphaeroides R-26: the cofactors. *PNAS* 84: 6438-6442.

Zouni A, Witt HT, Kern J, Fromme P, Norbert Krauss N, Saenger W and Orth P (2001) Crystal structure of photosystem II from *Synechococcus elongatus* at 3.8 Å resolution. *Nature* 409: 739-743.

VII. Tables

Table 1: Characteristics of the component bands and PSI/PSII stoichiometries originated from PSII (F685 and F695) and PSI (F_{PSI}) of 77K fluorescence emission spectra.

Cells	F685		F695		F_{PSI}		PSI%[b]	PSII%[c]	PSI/PSII[d]
	λpeak (nm)	Area[a] unit	λpeak (nm)	Area[a] units	λpeak (nm)	Area[a] (%)			
WT	686	23.7	698	18.4	718	57.9	57.9%	42.1%	1.38
4134	686	24	696	44	715	32	32%	68%	0.47
1042	684	48	698	32	717	20	20%	80%	0.25
4151	688	21.9	-	-	710	78.1	78.1%	21.9%	3.57
1051	688	9.1	-	-	710	91	91%	9.1%	10

[a]The abundance values were expressed as percentage of the sum of three emission bands (F686 + F696 + F_{PSI}); [b]The abundance percentage of PS I was calculated as F_{PSI}/(F686 + F696 + F_{PSI}); [c]The abundance percentage of PS II was calculated as (F686 + F696)/(F686 + F696 + F_{PSI}); [d]The ratio of PSI/PSII was calculated as F_{PSI} / (F686 + F696) on the assumption that each PS I contains the fluorescence bands between F710-735 and each PSII contains two fluorescence bands (F686 and F696).

Table 2: The summary of energy storage efficiencies.

	WT	4134	1042	4151	1051
ES	36%	64%	37%	76%	85%

VIII. Figures

Figure 1: The spectrophone (from Lüscher 1984, reproduced from Bell 1880).

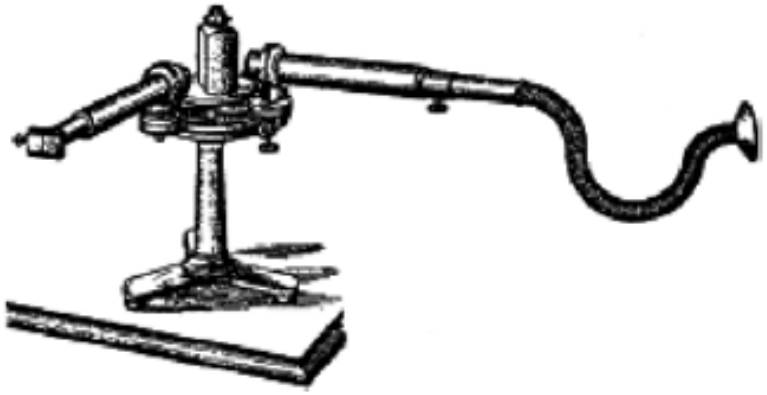

Figure 2: Principle of photoacoustic experiments.

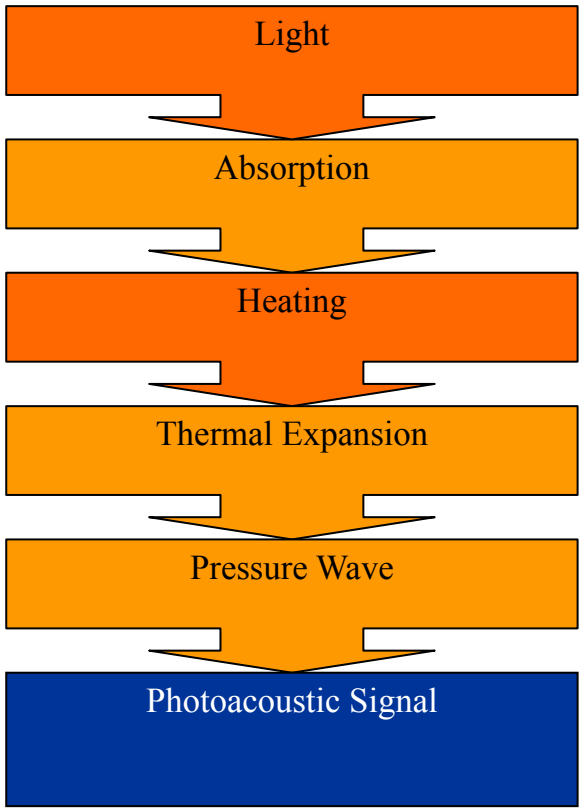

Figure 3: Schematic design of the photoacoustic experimental system: L, LEDs; S, beam shaping slits; BS, beam splitter; PAC, PA sample cell; SD, stainless-steel PA detector, containing a 10-mm diameter resonating ceramic disc; P, low noise Amtek preamplifier; A, low noise Ithaco 1201 amplifier; PD, photodiode; TS, trigger signal; BL, background light source (quartz-halogen illuminator); O, Tektronix TDS 430A oscilloscope; C, computer (based on fig.1 of Pinchasov et al. 2007).

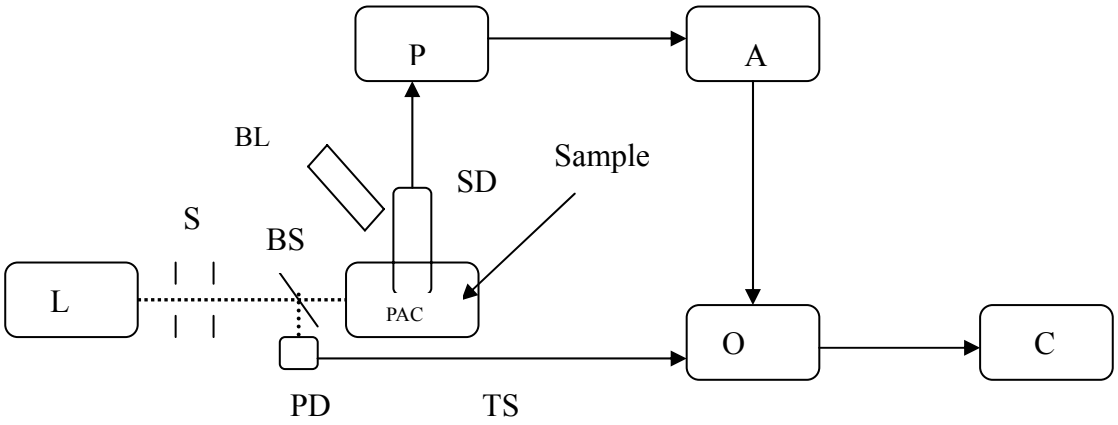

Figure 4: Photoacoustic system (corrected from the photos captured by Dr. Gorbunov)

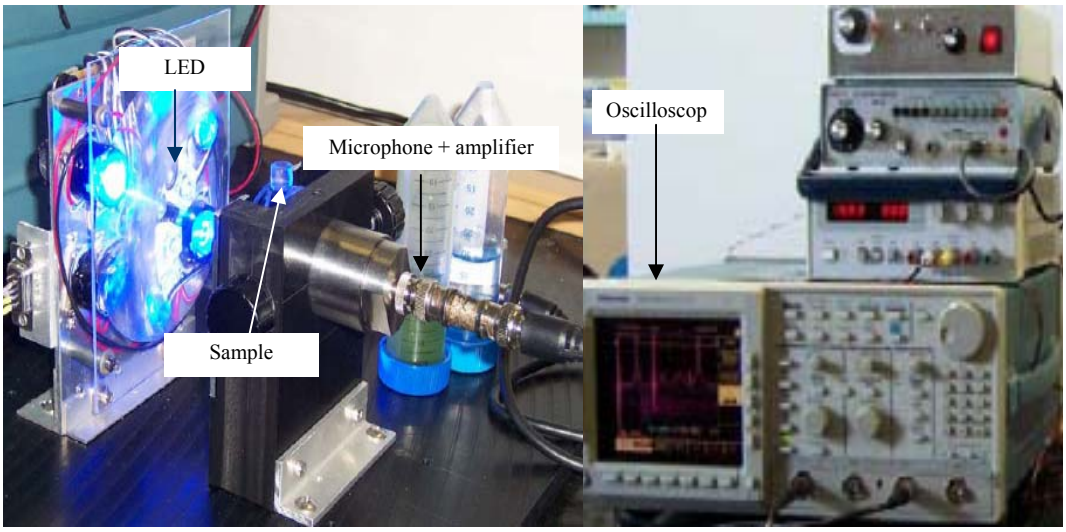

Figure 5a: Deconvolution analysis of 77 K fluorescence emission spectra of *C. reinhardtii* wild type cell (CC-125) fitted to Gaussian components. Fluorescence emission spectra were measured with excitation at 435 nm. Histograms on the top showed the unit which was directly calculated from the area under the curve of the individual component; solid lines in the middle were deconvoluted curves and their sum; the bottom of the histograms showed the residuals between the measured spectra and the best fit. The spectrum was normalized to the maximal activities (r^2= 0.98183359).

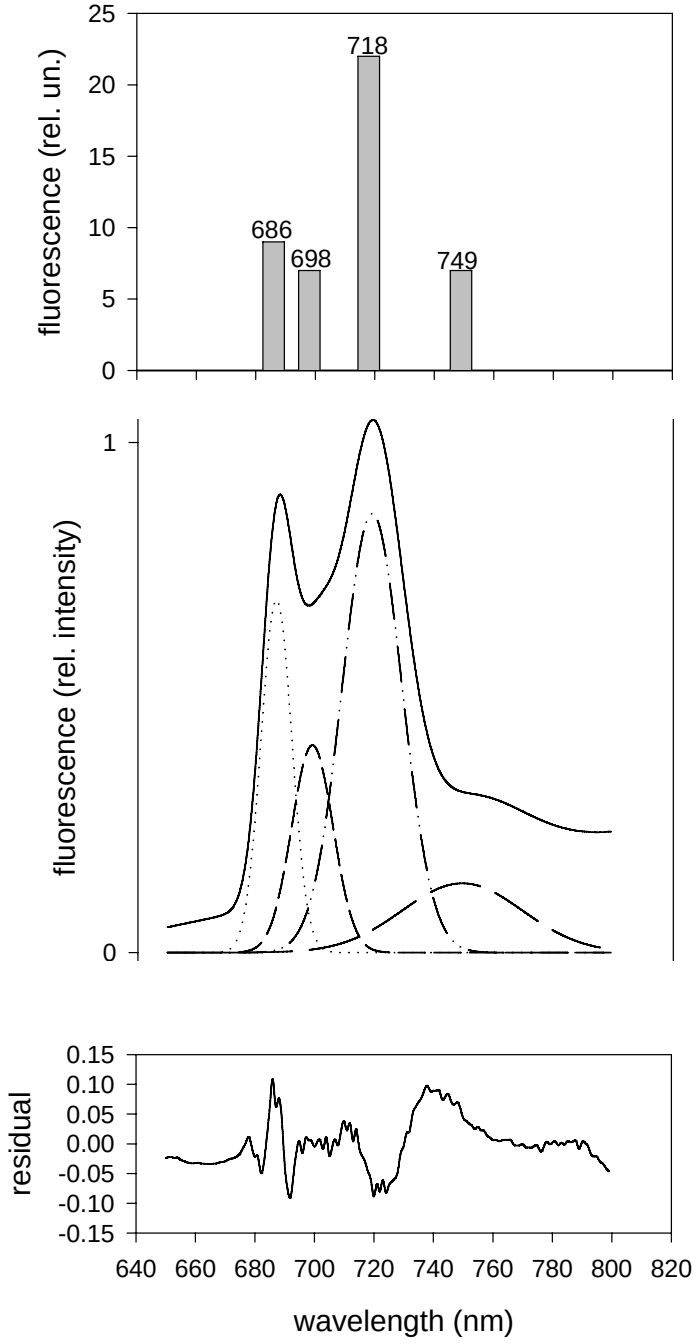

Figure 5b: Deconvolution analysis of 77 K fluorescence emission spectra of *C. reinhardtii* PSI-less mutant (CC-4134) fitted to Gaussian components. Fluorescence emission spectra were measured with excitation at 435 nm. Histograms on the top showed the unit which was directly calculated from the area under the curve of the individual component; solid lines in the middle were deconvoluted curves and their sum; the bottom of the histograms showed the residuals between the measured spectra and the best fit. The spectrum was normalized to the maximal activities (r^2= 0.994758).

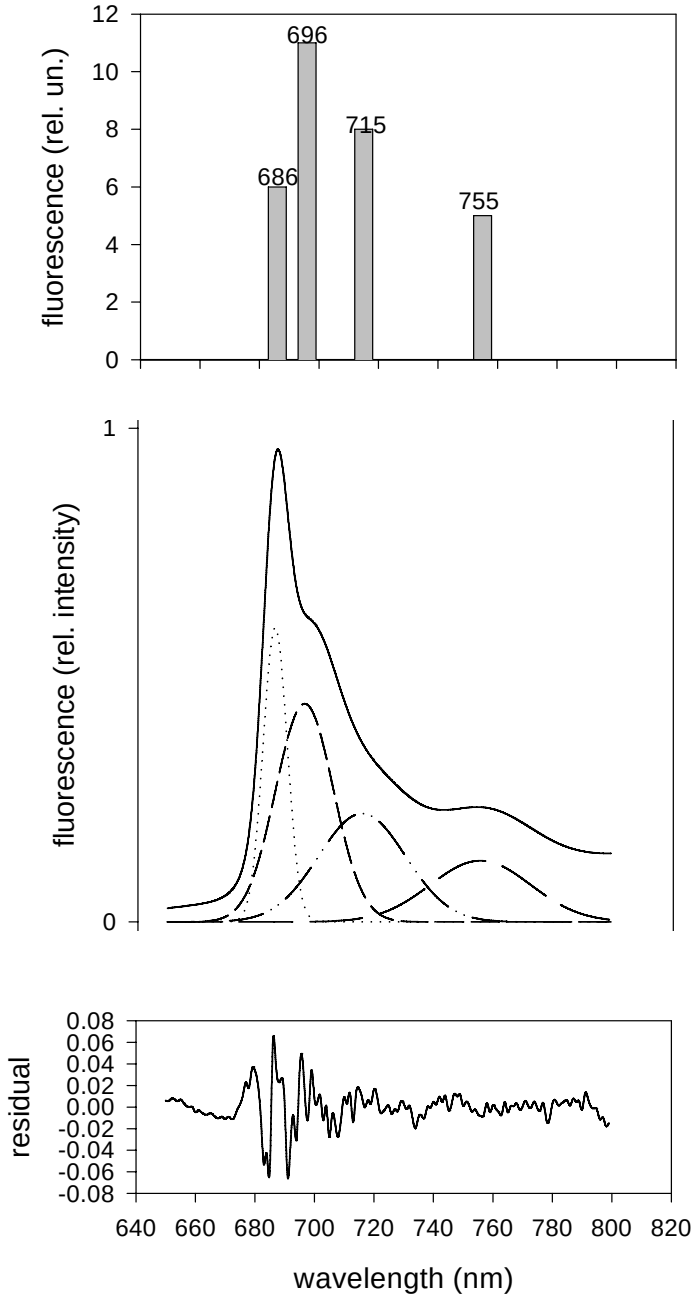

Figure 5c: Deconvolution analysis of 77 K fluorescence emission spectra of *C. reinhardtii* PSI-less mutant (CC-1042) fitted to Gaussian components. Fluorescence emission spectra were measured with excitation at 435 nm. Histograms on the top showed the unit which was directly calculated from the area under the curve of the individual component; solid lines in the middle were deconvoluted curves and their sum; the bottom of the histograms showed the residuals between the measured spectra and the best fit. The spectrum was normalized to the maximal activities (r^2= 0.995549).

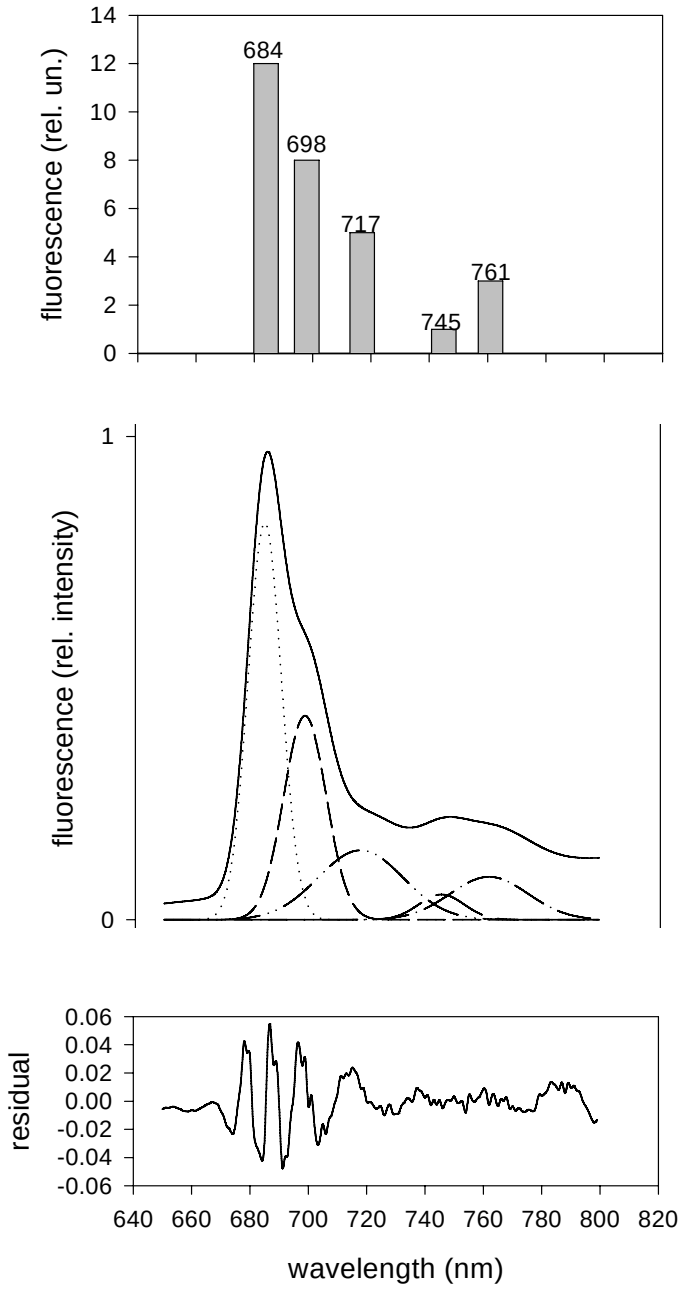

Figure 5d: Deconvolution analysis of 77 K fluorescence emission spectra of *C. reinhardtii* PSII-less mutant (CC-4151) fitted to Gaussian components. Fluorescence emission spectra were measured with excitation at 435 nm. Histograms on the top showed the unit which was directly calculated from the area under the curve of the individual component; solid lines in the middle were deconvoluted curves and their sum; the bottom of the histograms showed the residuals between the measured spectra and the best fit. The spectrum was normalized to the maximal activities (r^2= 0.989382).

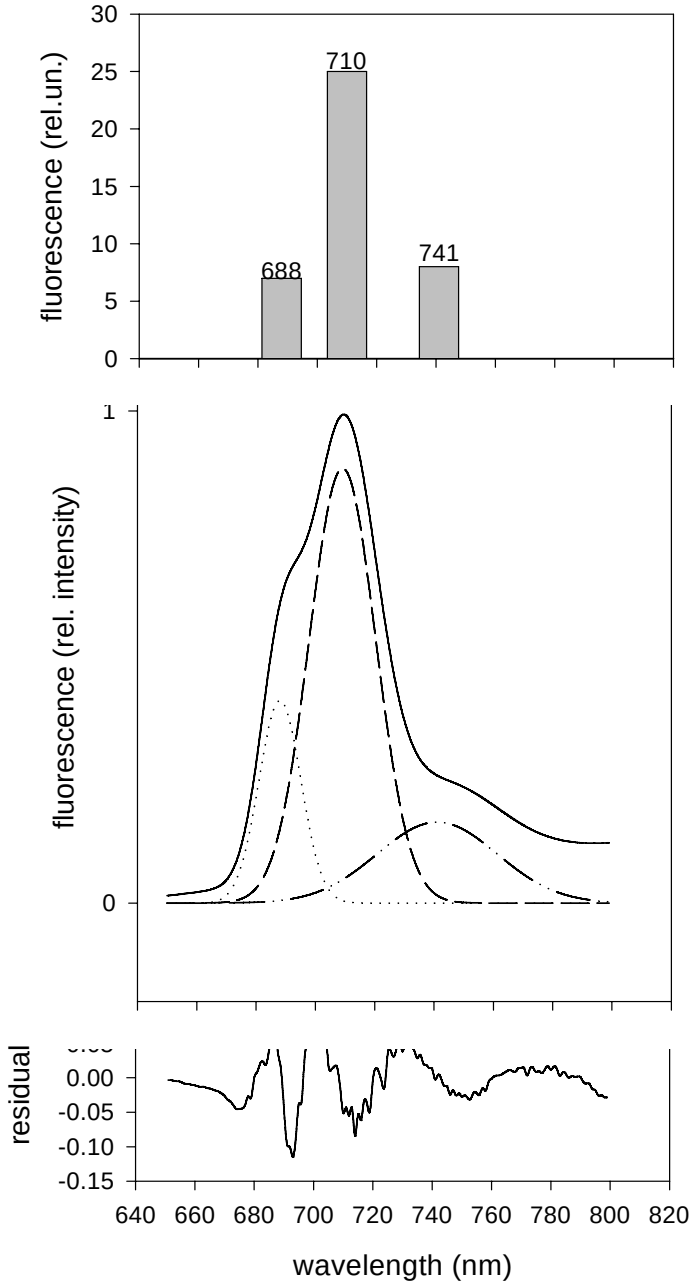

Figure 5e: Deconvolution analysis of 77 K fluorescence emission spectra of *C. reinhardtii* PSII-less mutant (CC-1051) fitted to Gaussian components. Fluorescence emission spectra were measured with excitation at 435 nm. Histograms on the top showed the unit which was directly calculated from the area under the curve of the individual component; solid lines in the middle were deconvoluted curves and their sum; the bottom of the histograms showed the residuals between the measured spectra and the best fit. The spectrum was normalized to the maximal activities (r^2=0.968266).

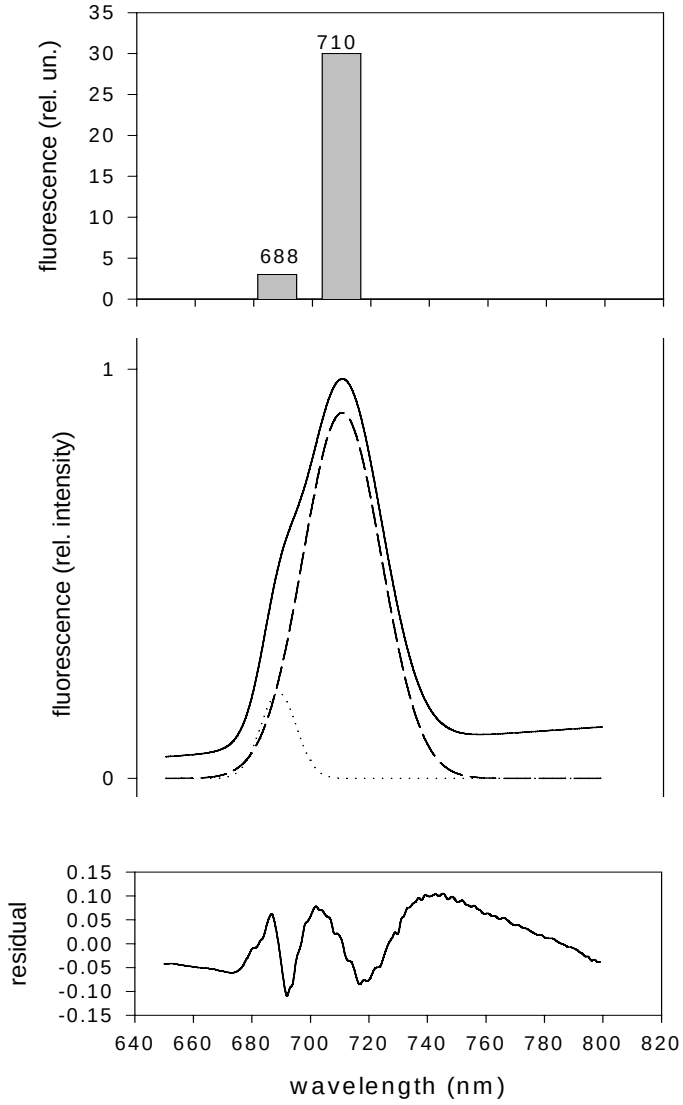

Figure 6: Photoacoustic spectrum of *C. reinhardtii* wild type cell. Curve 1, 25 °C, closed RCs, saturation continuous background light; curve 2, weak pulse light, ~4°C; curve 3, weak pulse light, 25 °C; curve 4, saturation continuous background light, ~4°C; curve 5, carbon ink solution, saturation continuous background light, 25 °C; curve 6, carbon ink solution, weak pulsed light, ~4 °C.

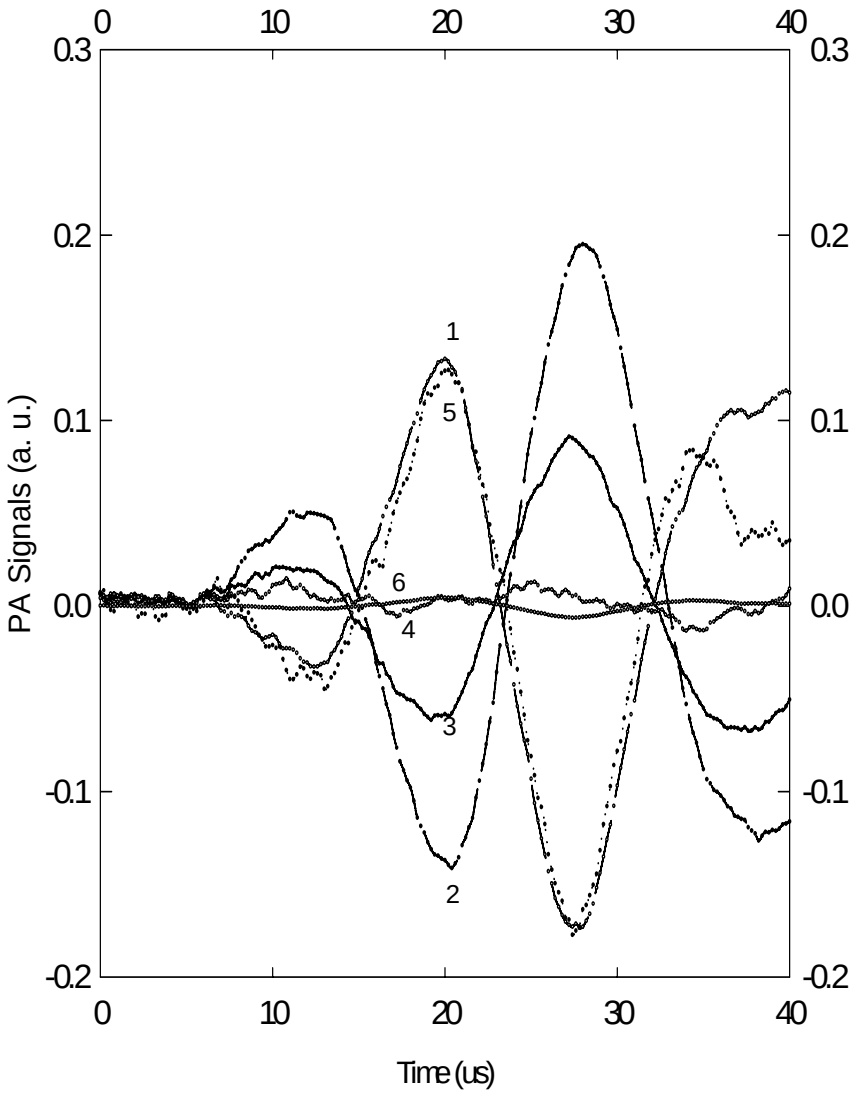

Figure 7a: Photoacoustic spectrum of CC-4134 (PSI-less mutant). Curve 1, saturation continuous background light, 25 °C; curve 2, weak pulse light, 4°C; curve 3, weak pulse light, 25 °C. All the data are corrected for the common "artifacts" and smoothed using FFT filter function of Origin 6.0 program.

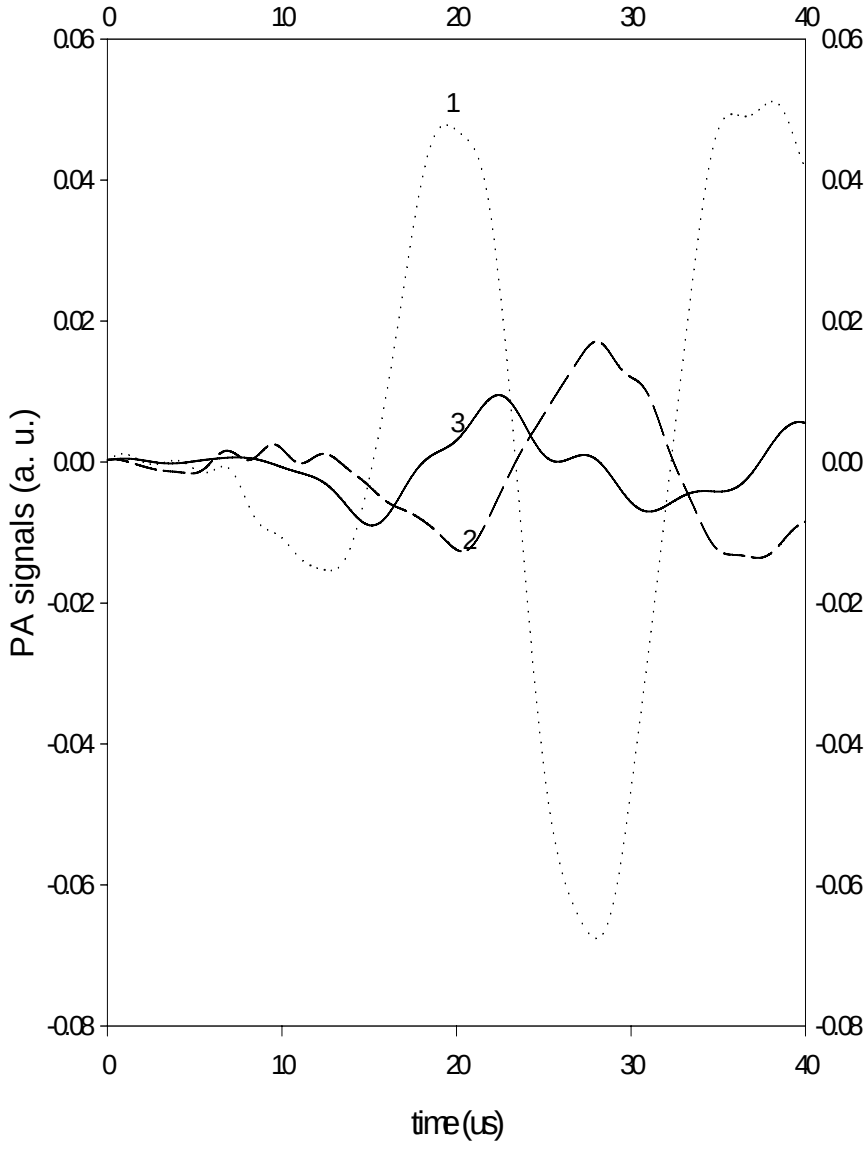

Figure 7b: PA spectrum of CC-1042 (PSI-less mutant). Curve 1, saturation continuous background light, 25 °C; curve 2, weak pulse light, 4°C; curve 3, weak pulse light, 25 °C. All the data are corrected for the common "artifacts" and smoothed using FFT filter function of Origin 6.0 program.

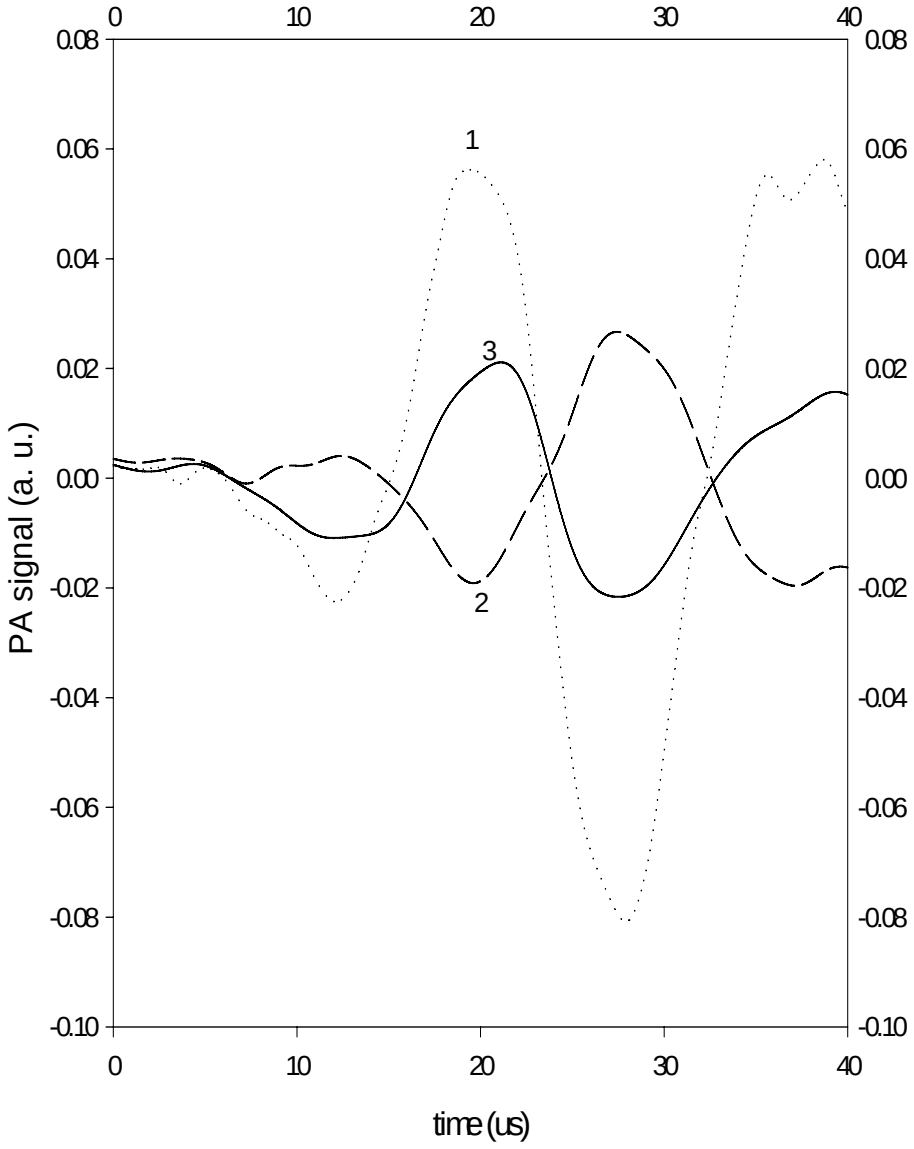

Figure 7c: PA spectrum of CC-4151 (PSII-less mutant). Curve 1, saturation continuous background light, 25 °C; curve 2, weak pulse light, 4°C; curve 3, weak pulse light, 25 °C. All the data are corrected for the common "artifacts" and smoothed using FFT filter function of Origin 6.0 program.

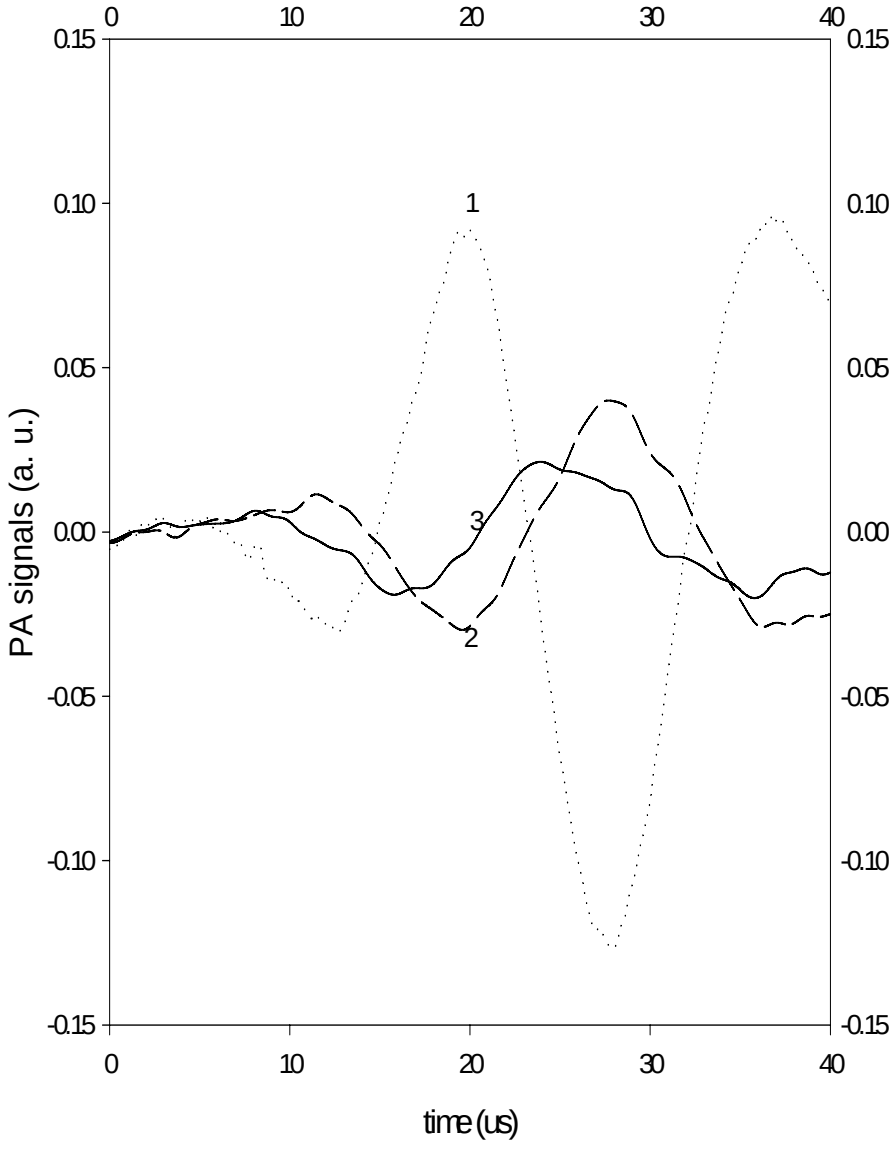

Figure 7d: PA spectrum of CC-1051 (PSII-less mutant). Curve 1, saturation continuous background light, 25 °C; curve 2, weak pulse light, 4°C; curve 3, weak pulse light, 25 °C. All the data are corrected for the common "artifacts" and smoothed using FFT filter function of Origin 6.0 program.

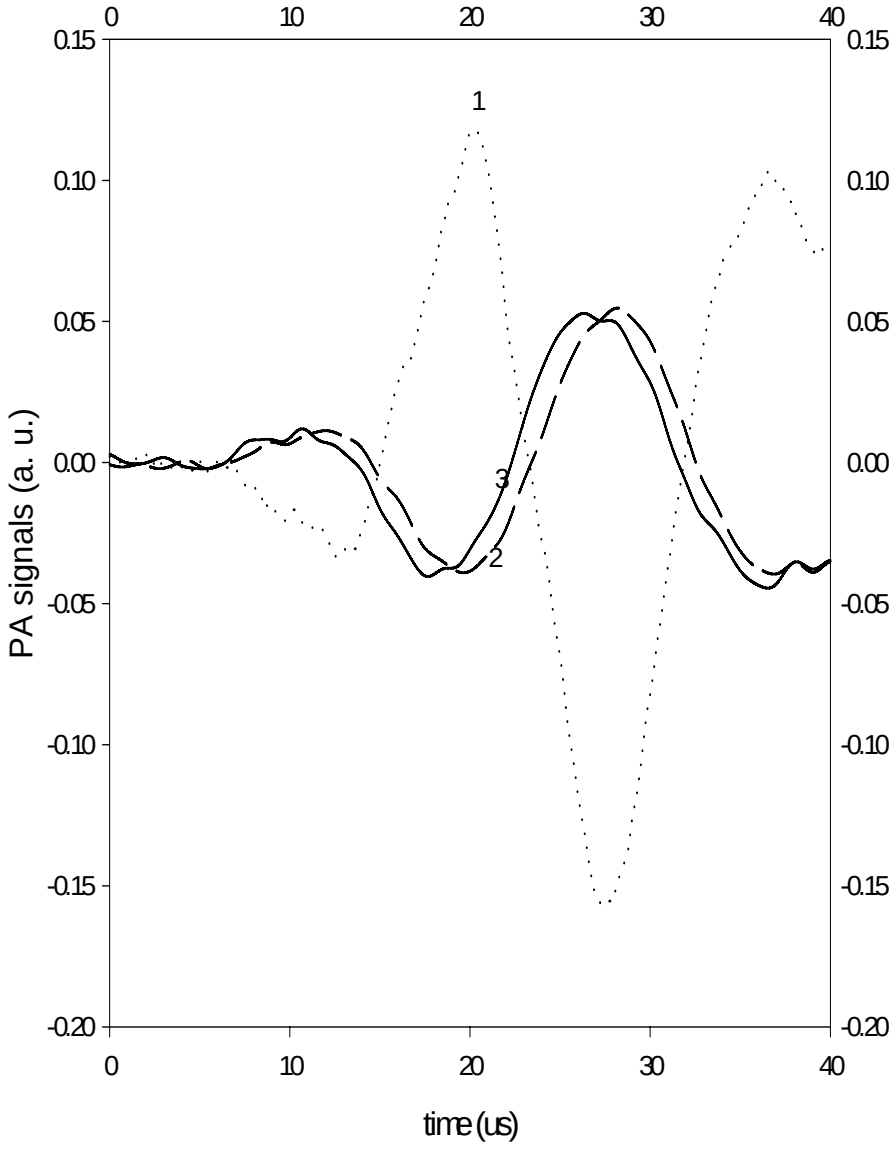

Figure 8a: Corrected PAo and PAm signals of WT (CC-125). Solid line is PAm; dash line is PAo. All data were normalized according to equation (2).

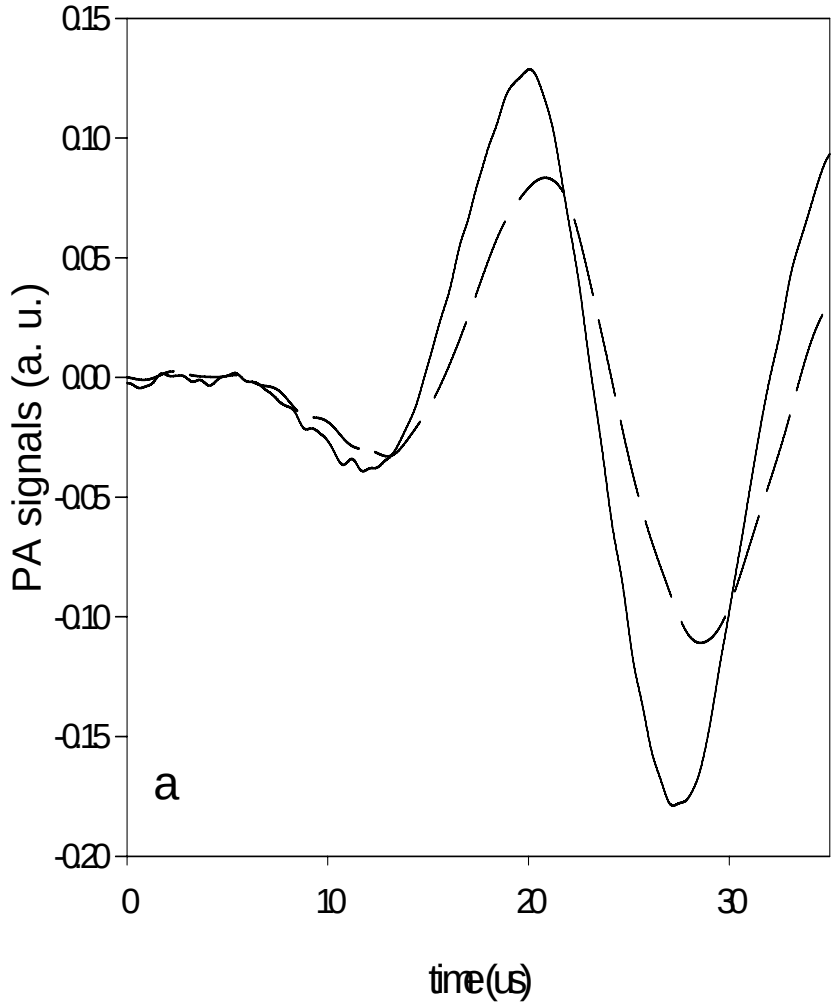

Figure 8b: Corrected PAo and PAm signals of PSI-less mutant (CC-4134). Solid line is PAm; dash line is PAo. All data were normalized according to equation (2).

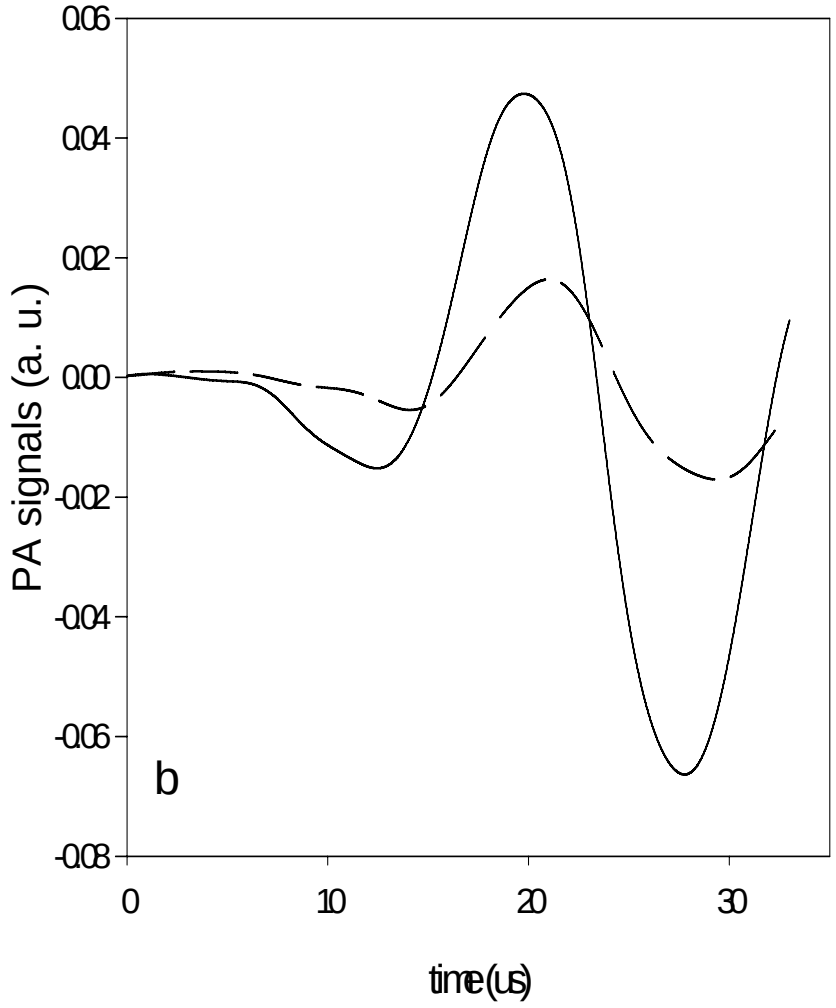

Figure 8c: Corrected PAo and PAm signals of PSI-less mutant (CC-1042). Solid line is PAm; dash line is PAo. All data were normalized according to equation (2).

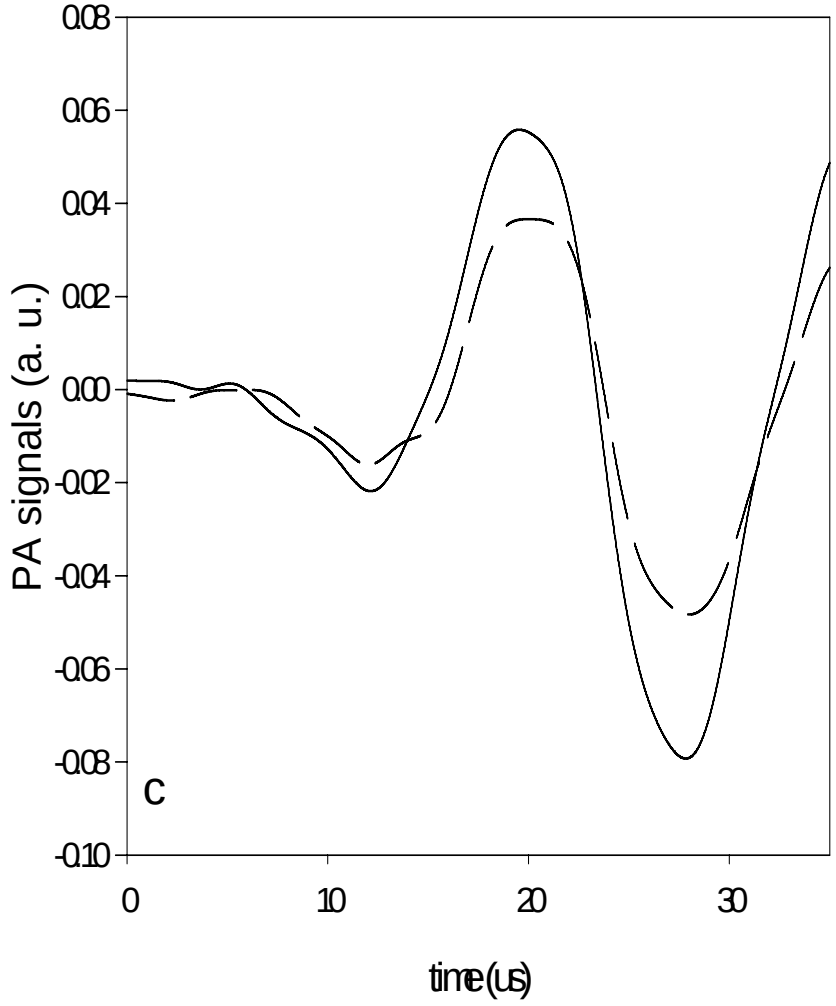

Figure 8d: Corrected PAo and PAm signals of PSII-less mutant (CC-4151). Solid line is PAm; dash line is PAo. All data were normalized according to equation (2).

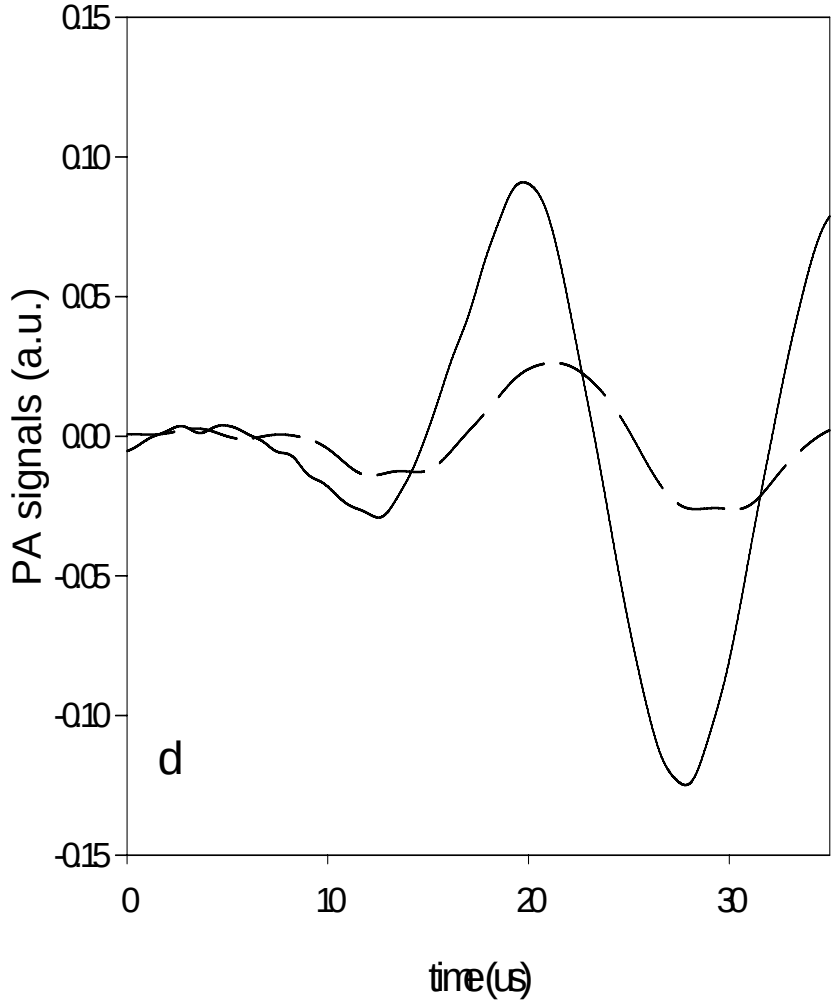

Figure 8e: Corrected PAo and PAm signals of PSII-less mutant (CC-1051). Solid line is PAm; dash line is PAo. All data were normalized according to equation (2).